②

REPORT DOCUMENTATION PAGE

1a. REPORT SECURITY CLASSIFICATION	1b. RESTRICTIVE MARKINGS
Unclassified	

2a. SECURITY CLASSIFICATION AUTHORITY	3. DISTRIBUTION/AVAILABILITY OF REPORT
2b.	Approved for public release: Distribution unlimited.

AD-A247 312

4. P	5. MONITORING ORGANIZATION REPORT NUMBER(S)
	AFOSR 92 0161

6a. NAME OF PERFORMING ORGANIZATION	6b. OFFICE SYMBOL (If applicable)	7a. NAME OF MONITORING ORGANIZATION
Emory University		AFOSR/NC

6c. ADDRESS (City, State and ZIP Code)	7b. ADDRESS (City, State and ZIP Code)
1515 Pierce Drive Atlanta, GA 30322	Building 410 Bolling AFB, DC 20332-6448

8a. NAME OF FUNDING/SPONSORING ORGANIZATION	8b. OFFICE SYMBOL (If applicable)	9. PROCUREMENT INSTRUMENT IDENTIFICATION NUMBER
AFOSR	NC	AFOSR-88-0249

8c. ADDRESS (City, State and ZIP Code)	10. SOURCE OF FUNDING NOS.			
Building 410 Bolling AFB, DC 20332-6448	PROGRAM ELEMENT NO.	PROJECT NO.	TASK NO.	WORK UNIT NO.
	61102F	2303	B1	

11. TITLE (Include Security Classification)
Relaxation dynamics of highly excited halogens in their electronic ground states

12. PERSONAL AUTHOR(S)
Michael Heaven

13a. TYPE OF REPORT	13b. TIME COVERED	14. DATE OF REPORT (Yr., Mo., Day)	15. PAGE COUNT
Final	FROM 8/1/89 TO 10/15/91	January 21, 1992	

16. SUPPLEMENTARY NOTATION

17. COSATI CODES			18. SUBJECT TERMS (Continue on reverse if necessary and identify by block number)
FIELD	GROUP	SUB. GR.	Chemical Lasers Halogens
			Metastable States Excimer Lasers
			Energy Transfer

19. ABSTRACT (Continue on reverse if necessary and identify by block number)

See additional page.

DTIC
ELECTE
MAR 1 0 1992
S D

···d for public ·lease,
·utior ·ted

20. DISTRIBUTION/AVAILABILITY OF ABSTRACT	21. ABSTRACT SECURITY CLASSIFICATION
UNCLASSIFIED/UNLIMITED ☑ SAME AS RPT. ☐ DTIC USERS ☐	Unclassified

22a. NAME OF RESPONSIBLE INDIVIDUAL	22b. TELEPHONE NUMBER (Include Area Code)	22c. OFFICE SYMBOL

DD FORM 1473, 83 APR   EDITION OF 1 JAN 73 IS OBSOLETE.

1. Characterization of the valence to ion-pair state transitions of I_2

Highly excited vibrational levels of ground state iodine, and all levels of the metastable $A^3\Pi(1_u)$ and $A'^3\Pi(2_u)$ states, are involved in processes leading to the dissociation of I_2 in the chemical oxygen iodine laser (COIL). Populations in these vibrationally and vibronically excited levels can be sensitively monitored by exciting laser induced fluorescence (LIF) from the valance to ion-pair transitions. However, accurate spectroscopic constants are required for the extraction of population distributions from spectral intensity data. Constants for the β-A and D'-A' systems were obtained from rotationally resolved spectra for jet-cooled, metastable I_2. Transitions from A, v"=0 to β, $25 \leq v' \leq 68$, and A', v"=0 to D', $21 \leq v' \leq 86$ were analyzed. RKR curves and Franck-Condon factors have been derived from this data.

2. Spectroscopy and Dynamics of Matrix Isolated I_2 and IBr

Studies of matrix isolated I_2 and IBr were undertaken in order to examine their electronic relaxation dynamics in simple cryogenic solids, and to determine the A and A' state radiative decay rates. For both I_2 and IBr, the B-X, A-X, and A'-X emission systems were characterized in Ar matrices. Fluorescence decay lifetimes were measured for the A and A' states. 193 nm excitation of IBr/Ar or I_2/Ar matrices resulted in emissions from the D'-A' transitions. Large matrix shifts were observed, caused by solvation of the excited state dipole. It is probable that an optically pumped laser, operating on the D'-A' transition of Ar matrix isolated I_2, could be constructed.

3. Electronic Spectroscopy of Open-Shell van der Waals Molecules

Van der Waals molecules which consist of a rare gas atom bound to a small free radical are, in many instances, potential excimer systems. In general, these complexes undergo a dramatic increase in binding energy, and decrease in bond length on electronic excitation. As a consequence of the large difference in excited and ground state potential surfaces, radiative electronic relaxation will favor transitions to the unbound region of the ground state. These properties are exploited in the most successful and familiar excimer lasers (e.g. ArF, KrF, XeCl etc). Electronic transitions of the van der Waals complexes AlAr, OH/D-Ar, OH/D-Ne, and CN-Ne were investigated with the long-term goal of assessing their laser potential. The OH/D-Rg complexes are of particular interest as they are iso-electronic with the rare gas fluorides. Rotationally resolved LIF spectra for these species provided information concerning the ground and electronically excited potential energy surfaces. Near UV transitions of AlAr and OH/D-Rg exhibited excimer characteristics.

CONTENTS.

92-05663

92 3 03 108

1. Characterization of the valence to ion-pair state transitions of I_2

1.1 Introduction

Highly excited vibrational levels of ground state iodine, and all levels of the metastable $A^3\Pi(1_u)$ and $A^3\Pi(2_u)$ states, are involved in processes leading to the dissociation of I_2 in the chemical oxygen iodine laser (COIL). Populations in these vibrationally and vibronically excited levels can be sensitively monitored by exciting laser induced fluorescence (LIF) from the valance to ion-pair transitions. The most useful transitions for this purpose are $D(0^+_u)$-$X(0^+_g)$, $\beta(1_g)$-$A(1_u)$, and $D'(2_g)$-$A'(2_u)$. The former has been well characterized by Ishiwata and Tanaka (1), and provides a convenient means for tracking populations in the high vibrational levels of $I_2(X)$. However, prior to the work described here, spectroscopic data for the β-A and D'-A' transitions were not suitable for monitoring populations in the lower vibrational levels of A and A'. In the previous studies, emissions from low vibrational levels of β or D' to high vibrational levels of A or A' were observed. The constants obtained by analyzing this data were not of sufficient quality for accurate prediction of the absorption or LIF spectra. Hence, LIF from the β-A and D'-A' systems had been observed in flowing mixtures of I_2 and $O_2(^1\Delta)$, but inversions of the intensity data to define population distributions could not be carried out (2). In order to obtain more accurate spectroscopic constants we have characterized the β-A and D'-A' transitions of jet-cooled I_2. This project was carried out in collaboration with Professor Joel Tellinghuisen (Vanderbilt University).

2

1.2 Experimental

The description of the experiment has been given elsewhere (3,4) and need only be recounted briefly here. A mixture of I_2 ($P \approx 0.3$ torr) and Ar (0.7 atm) was expanded through a 300 μm-diameter nozzle into a chamber which was evacuated by a Roots blower. The expanding gases were excited by 193-nm light from an ArF laser (Lumonics TE860-4) about 1 mm away from the nozzle, and were probed with a frequency-doubled tunable dye laser (Lambda Physik EMG101/FL3002E) 5-10 nozzle diameters downstream from the ArF laser beam. This laser was fired 3-5 μs after the ArF laser for proper synchronization. LIF was detected at 338-342 nm using a 0.25-m monochromator (Jarrell-Ash 82-410, $f/3.5$) equipped with a photomultiplier (EMI 9558QB). Long-pass filters (295-nm or 320-nm) further discriminated against scattered 193-nm and probe laser light. The signal was recorded by a transient digitizer (LeCroy TR8837F, 32 MHz sampling rate). The spectra were calibrated by simultaneously recording the I_2 B-X excitation spectrum obtained by directing the dye laser fundamental beam into an I_2 cell. A typical spectrum contained 400-600 points at intervals of 0.013 cm^{-1} (in first order).

Although the details of the mechanism for producing the A and A' states are still under investigation, the rationale for the experiment is as follows (5,6): Excitation of I_2 at 193 nm excites the very strong $D(0^+_u)$-$X(0^+_g)$ transition. Through collisions with Ar the D state then very rapidly interconverts and equilibrates with D', β, and other ion-pair states in the first cluster, all of which relax to low v' levels (7,8). Subsequent radiative decay of these states

populates intermediate v" levels in *A'* and *A*. Further collisions relax these states to low v"— the v" = 0 levels being the only levels detectable in the present experiments.

The use of the 340-nm setting for the fluorescence ensures that all v' levels of both the *D'* and the β states will be detected. This is because both the *D'* → *A'* and β → *A* systems have their long-wavelength extrema in this region (8) — a consequence of the minima in the respective difference potentials occurring near 29400 cm^{-1} (9). For the v' levels studied here the fluorescence in this region is bound-free.

The *B* ← *X* calibration lines were identified with the aid of the Gerstenkorn and Luc atlas (10). Line positions were estimated by simple 3-point parabolic fits about the peaks. Typical spectra contained 20-50 identified and resolved calibration peaks, which could be represented adequately by a fit linear (or rarely, quadratic) in wavenumber. Standard deviations of such fits were 0.003-0.005 cm^{-1} in first order.

1.3 Results

For both the β-*A* and *D'*-*A'* systems the conditions of the jet led to limited ranges of populated rotational levels in the initial state, consistent with a rotational temperature of about 5 K. This meant that even at the fairly narrow 0.08-cm^{-1} bandwidth of the probe laser, the spectra remained extremely congested (3,11,12). Typical examples of the rotational contours are shown in Figures 1 and 2.

4

Calib.

$I_2 \beta \leftarrow A$
37-0 Band

Exp.

Calc.
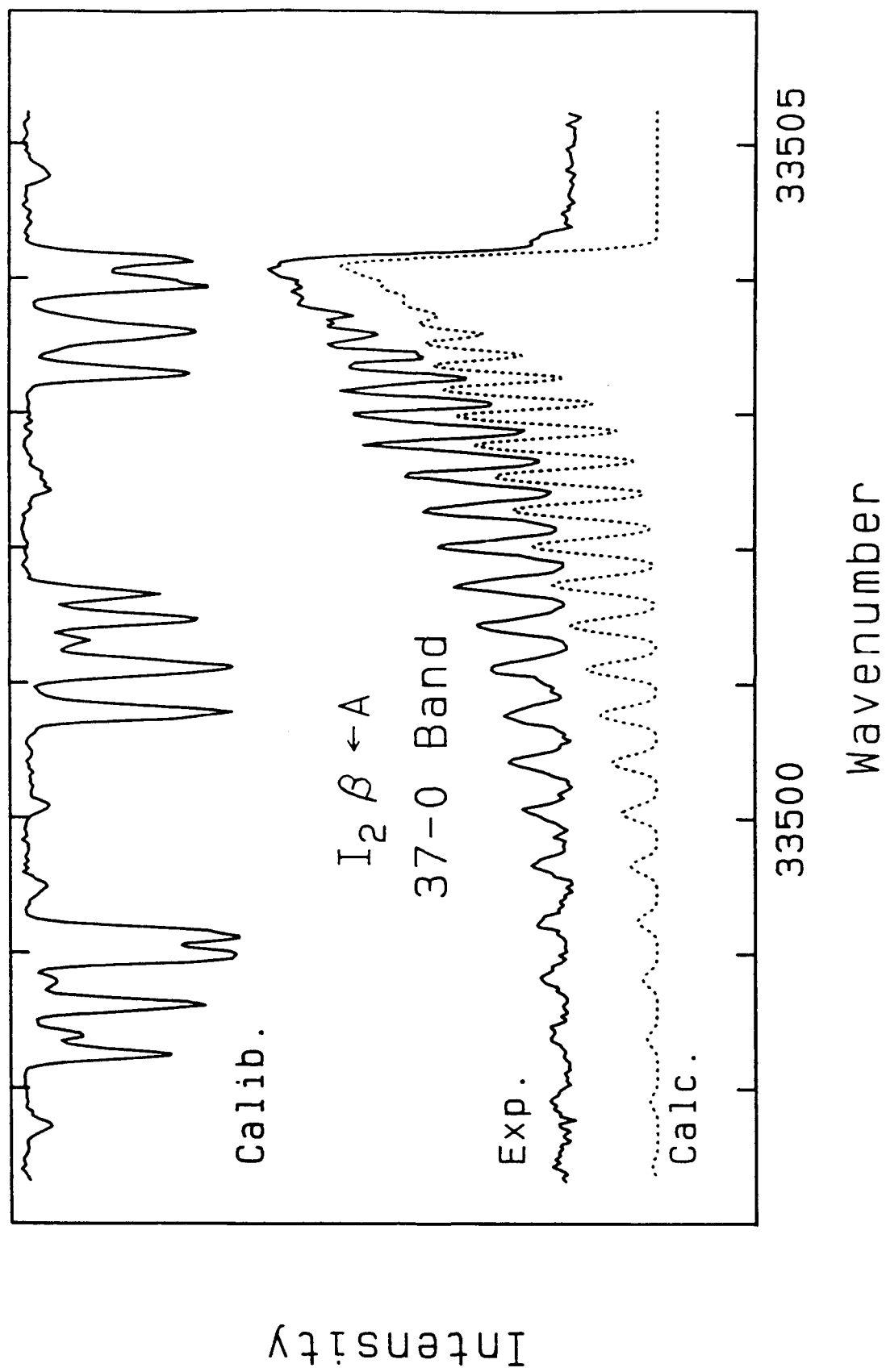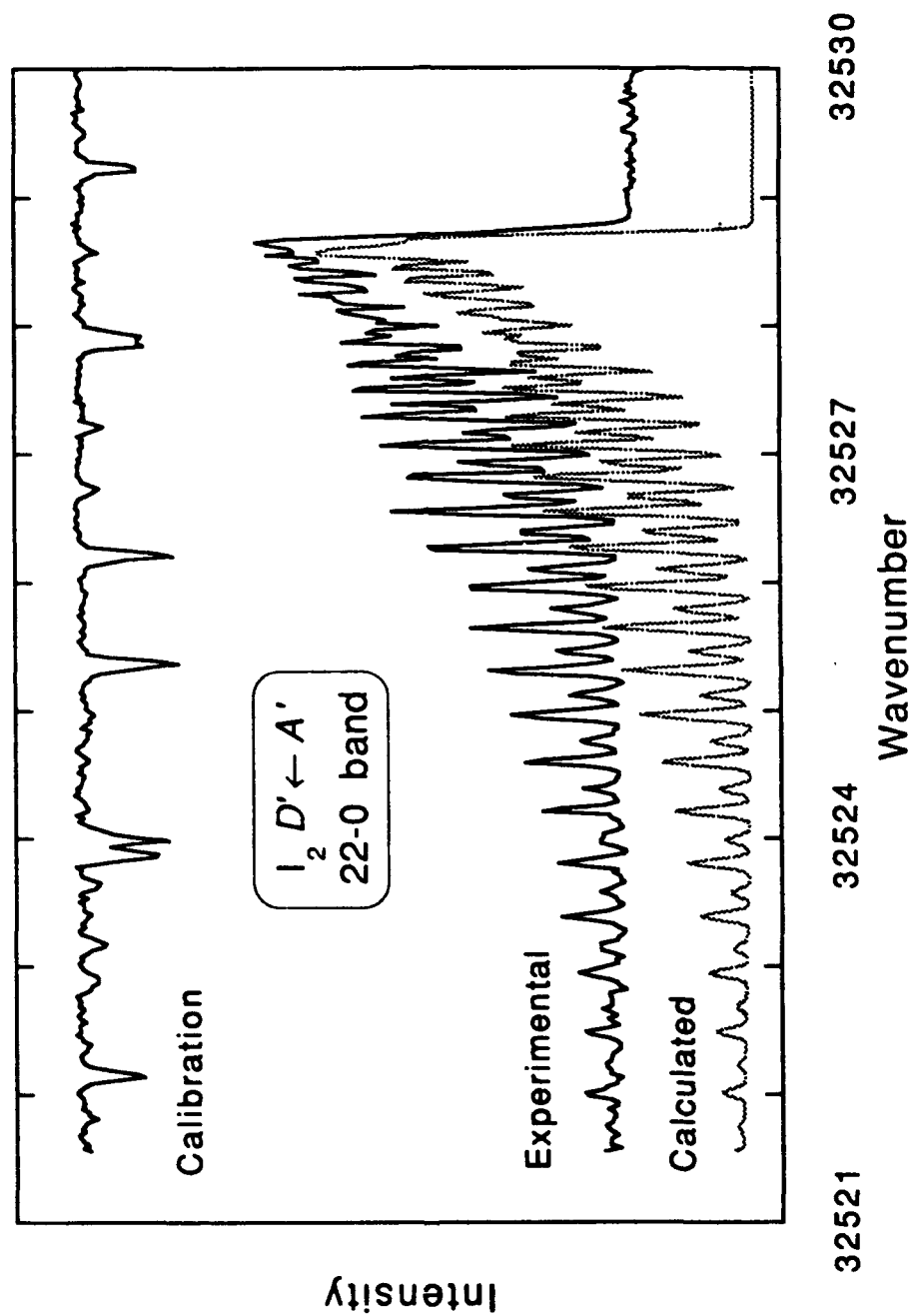
Intensity

Wavenumber

33500   33505

Figure 1.

Figure 2.

These congested spectra did not permit analysis by the usual "measure, assign, and fit" procedures of conventional high-resolution spectroscopy. Instead we developed a nonlinear fitting method for analyzing the observed band contours, including the unknown spectroscopic constants among the adjustable parameters of the fit. Details of this procedure are given in references 3, 11, and 12. Examples of contours generated from fitted parameters are shown in Figs 1 and 2. The primary spectroscopic constants determined from each contour were the ground and excited state rotational constants, and the band origin. Tables 1 and 3 list the constants determined for the β-A and D'-A' systems, respectively.

Results from the band-by-band analyses were utilized as the input to correlated least-squares fits, in order to extract global parameters for the ion-pair states, and the best estimates for the B_0'' constants. This type of merging procedure requires the constants and their associated variance-covariance matrices. Consequently, the latter are included in Tables 1 and 3. Molecular constants from the merged fits are given in Tables 2 and 4. RKR curves for the β and D' states, and Franck-Condon factors for the β-A and D'-A' systems, calculated using the new constants, are available on request. These results can be used for reliable inversion of intensity data.

5

Table 1

Origins, rotational constants, and variance-covariance matrices
from least-squares analyses of v'-$0''$ bands in the $\beta \leftarrow A$ spectrum of I_2 [a]

v'	ν_0	$B' \times 10^2$	$B'' \times 10^2$	$V_{11} \times 10^6$	$V_{12} \times 10^7$	$V_{13} \times 10^7$	$V_{22} \times 10^8$	$V_{23} \times 10^8$	$V_{33} \times 10^8$
25	32403.9903	1.9055	2.7287	1.9049	0.0614	0.1507	0.1041	0.1004	0.1062
26	32497.8785	1.8983	2.7245	1.2451	0.0807	0.1285	0.0522	0.0539	0.0604
27	32591.3458	1.8893	2.7211	0.8167	0.0497	0.0767	0.0379	0.0390	0.0445
28	32684.4184	1.8869	2.7243	1.8633	0.1398	0.1988	0.0712	0.0759	0.0887
30	32869.3355	1.8705	2.7162	2.9661	0.2337	0.3560	0.1363	0.1451	0.1671
31	32961.2020	1.8773	2.7291	1.7348	0.1247	0.2044	0.1087	0.1144	0.1307
33	33143.7572	1.8377	2.7059	4.5232	-0.1085	0.0644	1.1058	1.0833	1.0733
34	33234.4288	1.8604	2.7326	5.2452	0.4179	0.6589	2.1714	2.0071	1.8814
36	33414.5916	1.8263	2.7081	3.4603	-1.3482	-1.1535	1.3408	1.2480	1.1678
37	33504.0849	1.8210	2.7095	1.9936	-0.4929	-0.3882	0.7009	0.6652	0.6363
38	33593.1903	1.8310	2.7209	2.0661	-0.4610	-0.3457	0.7161	0.6796	0.6511
39	33681.9234	1.8160	2.7122	6.0385	-3.5728	-3.2227	3.6536	3.4237	3.2157
40	33770.2563	1.8087	2.7096	9.3477	-7.2166	-6.6542	7.3002	6.8473	6.4310
41	33858.2113	1.8244	2.7300	5.6680	-3.4820	-3.1437	3.7181	3.5031	3.3112
42	33945.7754	1.8026	2.7164	4.9329	-3.0297	-2.7804	2.8182	2.6522	2.4999
43	34032.9526	1.8030	2.7175	7.1180	-3.7819	-3.3595	3.9447	3.6933	3.4700
44	34119.7711	1.8062	2.7249	15.8367	-11.6587	-10.7379	11.3646	10.6533	10.0001
45	34206.1986	1.8008	2.7249	12.5766	-8.4227	-7.6838	7.8424	7.3066	6.8173
46	34292.2462	1.7842	2.7137	6.4351	-2.2381	-1.8240	2.0469	1.8864	1.7593
48	34463.2403	1.7719	2.7095	6.3252	-1.8043	-1.4520	1.8706	1.7621	1.6803
49	34548.1685	1.7866	2.7379	6.1847	-1.9027	-1.4614	1.3445	1.1831	1.0613
50	34632.7441	1.7627	2.7139	4.1607	-0.1790	0.0772	0.2969	0.2794	0.2839
51	34716.9324	1.7631	2.7212	4.1377	0.0100	0.2866	0.2326	0.2274	0.2494
52	34800.7553	1.7599	2.7235	4.4655	0.2193	0.4951	0.1785	0.1966	0.2414
65	35857.8151	1.6994	2.7266	3.2578	0.1398	0.3017	0.1372	0.1465	0.1683
66	35936.6653	1.6909	2.7220	1.8761	0.0339	0.1023	0.0650	0.0671	0.0732
68	36093.3693	1.6914	2.7381	2.9626	-0.0397	0.1398	0.2920	0.3001	0.3243

[a]Units cm^{-1} for origins and rotational constants, cm^{-2} for V .

Table 2

Spectroscopic Parameters (cm^{-1}) from correlated fit of $\beta \leftarrow A$ Spectrum of $I_2{}^{a}$

	$G_v{}'$	$B_v{}'$
c_0	$29\ 867.796(63)^{b}$	$0.0204\ 207^{c}$
c_1	105.029^{c}	$-5.62(7)\times 10^{-5}$
c_2	$-0.226\ 564(359)$	$5.3(9)\times 10^{-8}$
c_3	$3.443(163)\times 10^{-4}$	
c_4	$-1.16(27)\times 10^{-6}$	
c_5	$6(2)\times 10^{-9}$	
$B_0{}''$		$0.027\ 239(15)$
χ^2/ν	13.8	2.85

^{a}Data span $v' = 25\text{-}68$, $v'' = 0$ only. Standard errors $(1\ \sigma)$ in parentheses.

$^{b}T_e{}' - T_0{}''$.

Table 3

Origins, rotational constants, and variance-covariance matrices
from least-squares analyses of v'-$0''$ bands in the $D' \leftarrow A'$ spectrum of I_2 [a]

v'	v_0	$B' \times 10^2$	$B'' \times 10^2$	$V_{11} \times 10^6$	$V_{12} \times 10^7$	$V_{13} \times 10^7$	$V_{22} \times 10^8$	$V_{23} \times 10^8$	$V_{33} \times 10^8$
21	32433.5560	1.9257	2.7886	5.9481	0.3527	0.5453	0.0888	0.1012	0.1220
22[c]	32528.5969	1.9334	2.8046	0.6773	0.0326	0.0569	0.0167	0.0179	0.0203
23[b]	32623.4634	1.9353	2.8143	1.2388	0.0633	0.1072	0.0233	0.0257	0.0303
24	32717.8362	1.8790	2.7703	10.9074	-2.5939	-1.9754	10.7600	9.8910	9.1245
25	32811.7993	1.9188	2.8051	1.4736	0.0669	0.1303	0.0502	0.0540	0.0622
26	32905.4109	1.9156	2.8076	4.9728	0.2674	0.4473	0.1746	0.1803	0.1964
27	32998.6354	1.9069	2.8033	6.7002	0.0851	0.3957	0.3560	0.3518	0.3704
28	33091.4782	1.9164	2.8199	10.6164	-0.4518	0.2144	1.9834	1.8321	1.7476
29	33183.9376	1.8871	2.7962	14.8038	-0.3925	0.1423	1.5835	1.5398	1.5224
30	33276.0240	1.8878	2.8013	14.1511	-6.5793	-5.5886	8.6557	7.9916	7.4138
31	33367.7491	1.8699	2.7910	3.4793	-2.0850	-1.9161	2.1208	2.0149	1.9182
32[b,c]	33455.9528	1.8579	2.7994	3.8554	-2.5398	-2.3496	2.2049	2.0748	1.9548
33	33550.0634	1.8623	2.7938	2.2631	-1.2477	-1.1359	1.0708	1.0059	0.9470
34	33640.6643	1.8649	2.8006	2.1930	-0.4019	-0.3104	0.4754	0.4558	0.4411
35	33730.8704	1.8724	2.8103	1.1677	-0.2983	-0.2415	0.3000	0.2850	0.2732
36	33820.7214	1.8581	2.8049	5.5576	-4.2158	-3.8778	3.9649	3.7017	3.4600
37	33910.2162	1.8686	2.8165	6.6147	-4.6279	-4.2376	4.0684	3.7862	3.5280
38	33999.3492	1.8437	2.7967	7.3101	-2.4869	-2.0052	1.9594	1.7768	1.6309
39	34088.1129	1.8707	2.8316	6.5879	-2.2767	-1.9046	1.7767	1.6228	1.4930
40	34176.4982	1.8329	2.7968	8.5547	-2.9336	-2.3899	2.5703	2.3397	2.1511
41[c]	34264.5702	1.8254	2.7984	8.2786	-0.2350	0.0482	0.4080	0.3868	0.3794
42	34352.2280	1.8170	2.7945	23.0794	-1.5078	-0.7292	1.3059	1.2072	1.1400
43	34439.5129	1.8235	2.8034	6.1571	-0.4553	-0.1815	0.4300	0.3946	0.3754
44	34526.4705	1.8111	2.7968	5.0200	0.0099	0.2401	0.1814	0.1801	0.1947
45	34613.0716	1.8118	2.8035	4.4861	0.0891	0.2555	0.1108	0.1132	0.1252
46	34699.3090	1.8058	2.7991	8.0842	-0.0426	0.2236	0.2432	0.2375	0.2473
47	34785.1885	1.8030	2.8042	6.9445	0.1865	0.3800	0.0905	0.0949	0.1086
59[b]	35788.6947	1.7608	2.8217	0.9631	0.0189	0.0642	0.0365	0.0380	0.0430
62[b]	36031.8758	1.7405	2.8159	1.3105	-0.0097	0.0529	0.0739	0.0735	0.0777
65	36272.0489	1.6887	2.7838	4.6888	-2.7045	-2.4773	3.0910	2.9515	2.8247
68	36509.2578	1.6692	2.7763	6.5347	-3.9784	-3.7631	4.5909	4.4607	4.3389
71	36743.5078	1.6829	2.8081	6.1169	-2.0709	-1.8163	2.4140	2.3364	2.2718
74	36974.8500	1.6863	2.8215	1.7760	-0.2020	-0.1401	0.2555	0.2497	0.2469
77[c]	37202.9630	1.6708	2.8170	1.6430	-0.4718	-0.3962	0.5592	0.5385	0.5224
80[b]	37428.9684	1.6537	2.8240	1.7036	-0.0732	0.0225	0.1628	0.1615	0.1678
83[b,c]	37606.6901	1.6262	2.7909	4.0510	-0.2775	-0.0755	0.3664	0.3564	0.3598
86	37871.8024	1.6148	2.8061	2.3849	0.0295	0.1544	0.0905	0.0950	0.1093

[a] Units cm^{-1} for origins and rotational constants, cm^{-2} for V .

[b] Omitted from final least-squares rotational fit.

[c] Omitted from final least-squares vibrational fit.

Table 4

Spectroscopic Parameters (cm^{-1}) for D' —A' Transition of I_2[a]

	D'	A'
ΔT_e	30346.19(10)	
c_{v0} (T_e)	40 388.24(10)[b]	10·042.05(14)[b]
c_{v1} (ω_e)	103.960(9)	108.285(85)
c_{v2} ($-\omega_e x_e$)	-0.208 04(27)	-1.152(20)
c_{v3}	$2.30(4)\times10^{-4}$	$-9.16(1.80)\times10^{-3}$
c_{v4}	$-9.5(1.7)\times10^{-8}$	$-1.7(7)\times10^{-4}$
c_{v5}		$9.8(1.0)\times10^{-6}$
σ^c	0.009	
c_{r0} (B_e)	$2.0563(17)\times10^{-2}$	$2.8134(14)\times10^{-2}$
c_{r1} ($-\alpha_e$)	$-5.61(8)\times10^{-5}$	$-1.79(3)\times10^{-4}$
c_{r2}	$5.6(8)\times10^{-8}$	$-6.2(2)\times10^{-6}$
R_e(Å)	3.5944(15)	3.0730(8)
χ^2/v^d	3.12	

[a] Data span $v' = 0$-86, $v'' = 0$-32. Standard errors (1 σ) in parentheses. Parameters have been rounded by a systematic procedure that preserves their accuracy

2. Matrix isolation studies of I_2 and IBr.

2.1 Introduction.

Population of the halogen and interhalogen A and A' states via dissociation-recombination events in rare-gas matrices has provided a valuable means for characterizing these metastable states (13-22). Gas-phase fluorescence decay lifetimes are difficult to measure for the A state, and they have never been reported for the A' states. In many instances, these lifetimes are easily determined in rare-gas matrices (13-22). The emissions originate from v'=0 levels which have poor Franck-Condon overlaps with near-by states, so the lifetimes are usually unaffected by non-radiative processes. Useful spectroscopic data may also be derived from matrix studies. In the gas-phase, the A' states are known mostly through observations of the D'-A' transitions (23-26). As these Ω=2 states cannot be directly accessed from the ground state, problems have been encountered in determining their absolute energies. Despite the inherent low-resolution of matrix spectra, characterizations of the $A' \rightarrow X$ systems in rare-gas solids have yielded reliable estimates for A' state term values (16,19,20,22,27,28).

Studies of matrix isolated I_2 and IBr were undertaken in order to examine their electronic relaxation dynamics in simple cryogenic solids, and to determine the A and A' state radiative decay rates. The D'-A' transitions of I_2 and IBr in Ar matrices were briefly investigated.

2.2 Experimental.

The matrix isolation unit used for this work has been described previously (22). Samples were prepared by mixing small amounts of the halogen with a large excess of the rare gas host. Typical dilution ratio were of the order of 1:1000 to 1:2500. Deposition was carried out with the mirror held at temperatures of 10 to 20 K.

For the greater part of this work, matrices were excited by pulses from either a frequency doubled YAG laser (532 nm), a tunable dye laser, or an excimer laser (308 or 193 nm). All pulses were of 10-15 ns duration. Fluorescence from the matrix was detected along an axis which was perpendicular to the laser beam. Long-pass filters were used to remove scattered laser light. The filtered fluorescence was focussed through the slits of a monochromator. Light emerging from the monochromator was detected by a liquid nitrogen cooled germanium device (ADC 403; 900-1600 nm) or a photomultiplier (RCA C31034A). Signals from the detectors were processed by a boxcar integrator (SRS 250) for the recording of fluorescence spectra and fluorescence decay curves in excess of 5 ms. Faster decays were captured in real time using a transient digitizer.

2.3 Summary of results for I_2 rare gas matrices

The I_2 A-X and A'-X emission systems were investigated in Ar, Kr, and Xe matrices (16). Lifetime measurements for $I_2(A)$ were consistent with radiative relaxation and a gas phase lifetime (after correction for the refractive index of the host) of 230±40 μs. The

fluorescence decay characteristics of $I_2(A')$ were found to be dependent on sample concentration and the means of excitation used. Radiative decay of $I_2(A')$ was observed when dilute samples were excited at 193 nm. A lifetime of 6 ± 1 ms was observed in Ar matrices. Excitation of $I_2(A')$ by dissociation-recombination channels yielded long-lived fluorescence decays. This effect was ascribed to slow transfer of population from initially excited metastable states into the A' state. The presence of molecules in metastable states other than A and A' was demonstrated by sequential two-photon excitation measurements. The concentration dependence of the A' state decay characteristics was interpreted in terms of perturbation facilitated transfer of population into $I_2(A')$.

The $D' \to A'$ emission spectrum was observed when I_2:Ar matrices were excited at 193 nm (16). Interaction with the host red-shifted the spectrum by 2900 cm^{-1} from its gas phase position. It is probable that an optically pumped laser, operating on the D'-A' transition of Ar matrix isolated I_2, could be constructed. Excitation of I_2:Kr matrices at 193 nm produced a broad emission centered at 423 nm. This could be assigned to D'-A', but the implied matrix shift would be unusually large. Alternatively, the 423 nm band could originate from a charge transfer complex such as KrI$^+$-I$^-$. Lasing of this transition may also be feasible.

2.4 Summary of results for IBr/Ar matrices

Visible laser excitation of IBr/Ar matrices resulted in fluorescence from the B, A, and A' states (28). The B-X emission spectrum, and the B state excitation spectrum were found to be

12

structureless. Efficient predissociation of all *B* state levels was inferred from relative quantum yield data. Matrix stabilization of the *B'* state was not observed.

Wavelength-resolved fluorescence spectra were recorded for the *A-X* and *A'-X* systems (28). Vibronic analyses of these spectra yielded ground state vibrational constants which were virtually identical to the gas-phase values. Electronic term energies of $T_e(A)=12130\pm30$ and $T_e(A')=11180\pm30$ cm^{-1} were determined. Radiative lifetimes of $\tau(A)=140\pm10$ μs and $\tau(A')=25\pm3$ ms were obtained from time-resolved fluorescence measurements. Comparisons with the corresponding results for other halogens and interhalogens suggest that the IBr *A* and *A'* states are unaffected by non-radiative decay processes in solid Ar. Excitation spectra were consistent with efficient transfer from *B*, *Y*, and $^1\Pi_1$ to the *A* and *A'* states.

Excitation of IBr/Ar matrices at 193 nm produced an emission feature at 419 nm. This has been tentatively assigned to the *D'-A'* transition, red-shifted about 2100 cm^{-1} relative to the gas-phase (28). This large red-shift is attributed to solvation of the excited state electric dipole.

3. Electronic Spectroscopy of Open-Shell van der Waals Molecules

3.1 Introduction

Van der Waals molecules which consist of a rare gas atom bound to a small free radical are, in many instances, potential excimer systems. In general, these complexes undergo a dramatic

13

increase in binding energy, and decrease in bond length on electronic excitation (29). This occurs because the binding in the ground state is predominantly mediated by dispersion forces, while the stability of the excited states may be enhanced by increased polarizability, charge transfer, and orbital overlap effects. As a consequence of the large difference in excited and ground state potential surfaces, radiative electronic relaxation will favor transitions to the unbound region of the ground state. These properties are exploited in the most successful and familiar excimer lasers (e.g. ArF, KrF, XeCl etc).

Electronic transitions of the van der Waals complexes AlAr, OH/D-Ar, OH/D-Ne, and CN-Ne were investigated with the long-term goal of assessing their laser potential.

3.2 Experimental

Radical-rare gas atom complexes were generated in free-jet expansions (29). A mixture containing stable precursor molecules, seeded in a large excess of the appropriate rare gas, was expanded through a 300 μm diameter nozzle. Radicals were generated by pulsed laser photolysis of the mixture in the early stages of expansion, where the gas density was high. Subsequently, the radicals experienced efficient collisional cooling and complex formation. The complexes were characterized in the downstream region of the expansion by LIF and wavelength resolved fluorescence techniques. The equipment used for this purpose was described in Section 1.2.

14

3.3 Summary of Results for Al-Ar

Al-Ar was studied in a collaborative effort with Professor James L. Gole (Georgia Institute of Technology). Al atoms were generated by 193 nm photolysis trimethyl-aluminum. The atoms and Al-Ar complexes were detected by LIF of the Al 4s $(^2S) \leftarrow 3p(^2P)$ transition (30). In the complex the Al atomic energy levels are perturbed by interaction with the Ar atom. Molecular $X^2\Pi$ and $A^2\Sigma^+$ states correlated with $3p(^2P)$, while a $B^2\Sigma^+$ state correlated with 4s (^2S). Near UV LIF spectra (392-397 nm) for jet-cooled Al-Ar showed a progression of six vibronic bands. These originated from $X^2\Pi_{1/2}$, $v''=0$, and terminated on the $B^2\Sigma^+$, $1 \leq v' \leq 6$ levels. Rotationally resolved spectra yielded band origins, rotational constants, and the ground state Λ-doubling constant. A merged fit to the constants produced the molecular parameters listed in Table 5. Information concerning the ground state was deduced from the zero-point rotational constant, and the shift of the complex spectrum relative to the atomic transition. For the B state, the range of levels observed was sufficient to define an accurate RKR curve. The turning points of this curve are given in Table 6.

The B-X spectra showed that the electronically excited state was substantially more tightly bound than the ground state. Upon electronic excitation the well-depth increased by a factor of 2.7, while the equilibrium internuclear separation decreased by 0.74 Å. These changes were consistent with the increase in polarizability that accompanied electronic excitation of the Al atom.

15

Table 5

Spectroscopic Constants for the *B* and *X* States of Al-Ar
(all values in cm^{-1}, except R$_e$ which is in Å)

Constant	X	B
B_e	0.0727(±5)	0.1124(±11)
α_e	0.0036(±5)	0.0011(±2)
γ_e	-	-0.00052(±5)
ω_e	31.6[a]	81.50(±1.55)
$\omega_e x_e$	1.51[a]	4.88(±0.78)
$\omega_e y_e$	-	0.51(±15)
$\omega_e z_e$	-	-0.045(±9)
D_e	180	440
R_e	3.79(±1)	3.05(±1)

a. C. L. Callender, S. A. Mitchell, and P. A. Hackett, J. Chem. Phys. 90, 5252 (1989)

Table 6

RKR Turning Points for AlAr(B)

v'	$G(v')/cm^{-1}$	$R_{min}/\text{Å}$	$R_{max}/\text{Å}$
0	40.01	2.902	3.220
1	116.18	2.799	3.378
2	185.86	2.738	3.513
3	249.97	2.697	3.648
4	308.30	2.670	3.794
5	359.59	2.651	3.963
6	401.49	2.631	4.183
7	430.56	2.589	4.527

3.4 Summary of Results for OH/D-Ar

OH/D-Ar complexes were formed in Ar expansions by 193 nm photolysis of H/DNO$_3$ vapor (31). Progressions of the intermolecular stretch and bend-stretch levels were seen in conjunction with the OH/D A-X 0-0 and 1-0 transitions. The qualitative features of the van der Waals progressions were independent of the monomer (OH/D) transitions. At low energies, dominant stretch progressions were seen. On the high energy side of each progression, anharmonic bend-stretch progressions gained intensity at the expense of the pure stretch bands. The rovibrational structures of the stretch bands were surprisingly simple, and superficially consistent with a pseudo-diatomic model. Excited state vibrational intervals gave excellent fits to the expression for a Morse oscillator. At a resolution of 0.08 cm^{-1}, the rotational energy levels were well-represented by linear molecule rigid rotor expressions for a Hund's case (b) $^2\Sigma^+$ excited state and a case (a) $^2\Pi_{3/2}$ ground state. Furthermore, the dependence of the A state rotational constant on the stretch quantum number (v_2) was consistent with a Morse potential. Deviations from this simple one-dimensional picture were indicated by the breakdown of conventional vibrational isotope relationships (31).

Vibrational assignments for the OH-Ar stretch bands were initially based on the numbering from a matrix study (32). Assignments for the OD-Ar spectrum, and the bend-stretch levels of OH-Ar, were established by fitting a two-dimensional intermolecular potential energy surface (IPS) to the measured vibrational intervals for OH/D(A, v=0)-Ar (33). An ab-initio IPS

18

was used as the starting point for these calculations (34). We calculated the eigenvalues of trial potential surfaces using a large direct product basis set. Systematic adjustment of the IPS resulted in accurate prediction of the measured vibrational spacings and rotational constants. The parameters of this surface are given in reference (33). The fitted potential presented barriers to internal rotation in the A state that were large compared to the monomer rotational constant. Consequently, the low energy librational levels were best described in terms of a linear molecule, wide amplitude bending model. The eigenvalues and wavefunctions of the fitted IPS have been used to assign all prominent features of the OH/D-Ar LIF spectra. An interesting inverse isotope effect was discovered in the process of fitting the IPS (33).

The depth of the A state IPS (D_e=1062 cm^{-1} for OH/D(v=0)-Ar) and the short equilibrium intermolecular separation (R_{2e}=2.80 Å) indicated an unusually strong interaction. Goodman and Brus (32) proposed that partial donation of electron density from Ar to the partially filled σ bonding orbital of OH/D(A) may be responsible for the strength of the bond. An electronic perturbation of this kind could be manifest as a modification of the radiative lifetime. However, we (35) found that the lifetime of OD(A, v=0)-Ar was unaffected by complex formation. Lifetimes for OH(A, v=0)-Ar were slightly shorter than that of OH(A, v=0), but this effect was attributed to a weak electronic predissociation (OH(A, v=0)-Ar→OH(X, v≈13)+Ar).

19

3.5 Summary of Results for OH/D-Ne

OH/D-Ne complexes were formed in Ne expansions by photolysis of H/DNO$_3$ vapor. Rotationally resolved LIF spectra for the A-X transition of OH/D-Ne were recorded for complex bands associated with the monomer 0-0, 1-0, and 2-1 transitions (36,37). Each monomer transition was accompanied by three or four OH/D-Ne features. The energy spread of the van der Waals progressions provided lower limits for the dissociation energy of $D_0' > 61.8$ cm^{-1} (OH(A, v_1=0)-Ne) and 68.5 cm^{-1} (OD(A, v_1=0)-Ne). An analysis of the rotational constant and band origin data showed that the A state IPS was weakly bound, with a low barrier to internal rotation. Hence, the angular momentum coupling corresponds to Dubernet et al's (38) case (B), and the hindered rotor levels may be labeled by the quantum numbers r (for OH/D rotation) and $\Re$ (the projection of r on the intermolecular axis). Using the notation (v_1, r$^\Re$, v_2) for levels of the A state, the prominent features associated with each monomer transition could be described as a sub-origin (v_1, 0^0, 0), a -Ne stretch fundamental (v_1, 0^0, 1), and two bend-stretch combination bands (v_1, 1^0, 1) and (v_1, 1^1, 1). Owing to the wide amplitude of the zero-point "bend", the -Ne stretch frequency was subject to a large inverse isotope effect. For example, the (0, 0^0, 1)-(0, 0^0, 0) intervals are 29.3 and 42.4 cm^{-1} for OH-Ne and OD-Ne, respectively. The anisotropy of the IPS was directly reflected in the (v_1, 1^1, 1)-(v_1, 1^0, 1) separations. These intervals could be reproduced using an effective angular potential of the form

$$V(\theta) = C_1 \cos \theta + C_2 (3\cos^2 \theta - 1)/2. \tag{1}$$

20

A fit to the $v_1=0$ levels was achieved using $C_1=-10$ and $C_2=-21.5$ cm^{-1}. Discrepancies between the measured and calculated $(0, 1^0, 1)$-$(0, 0^0, 1)$ intervals resulted from the neglect of bend-stretch coupling. Stretch-stretch interactions were found to be weak. The OH(A) $v_1=0$ to 1 vibrational interval was reduced by only 3 cm^{-1} in the complex.

Due to the weakness of the intermolecular interaction, vibrational predissociation of OH/D(A, $v_1=1$)-Ne was slow enough to be observed in the real time fluorescence decay dynamics. Predissociation rates in the range of $(2\text{-}6)\times10^5$ s^{-1} were observed, with no recognizable isotopic dependence. Wavelength-resolved fluorescence spectra showed emission from both the complex and the photofragments. For OH-Ne, vibrational predissociation left OH(A) in $v_1=0$, N=12, which was the highest energy rotational level which could be populated. Predissociation of the OD(A)-Ne $(1,0^0,1)$ and $(1,1^1,1)$ levels populated N=15, but this product state was not energetically accessible from $(0,0^0,0)$. Consideration of the energetics governing OD-Ne predissociation placed limits of $76 < D_0' < 112$ cm^{-1} on the dissociation energy. The lack of isotopic dependence of the vibrational predissociation rates was consistent with the strong preference for channeling the excess energy into fragment rotation. The rates themselves were remarkably close to the average vibrational relaxation rates measured (39) for OH/D(A, $v_1=0$) in solid Ne ($k_{1-0}=0.9\times10^5$ s^{-1} and 0.4×10^5 s^{-1} for OH and OD, respectively). Based on the relatively small isotopic dependence of the relaxation rate, Brus and Bondybey (39) concluded that relaxation in solid Ne proceeded via vibration to rotation transfer.

Thus, it appears that significant features of the solid phase relaxation dynamics are reflected in the behavior of the binary complex.

Electronic predissociation of low rotational levels of $OH(A, v_1=2)$ is known to occur at rates in the range of $(4.7-6.4) \times 10^6$ s^{-1} (40). However, fluorescence decay rates (37) for the OH-Ne $(2, r^{\mathfrak{R}}, v_2)$ levels were found to be <u>slower</u> than those for $OH(A, v_1=2)$. Apparently, the presence of the Ne atom diminished the electronic predissociation rate by obstructing escape of the H atom. In accordance with this picture the levels with $\mathfrak{R}=0$, where there is a high probability of finding the Ne atom on the OH axis, predissociated less rapidly than the $\mathfrak{R}=1$ level, where the librational wavefunction has a node at the linear geometry. Physical obstruction of the predissociation also slows the fluorescence decay rate of $OH(A, v_1=2)$ in solid Ne (39).

3.6 Summary of Results for CN-Ne

The $B^2\Sigma^+$-$X^2\Sigma^+$ transition of CN provides a convenient means for detecting CN-Ne complexes. Three bands of the complex, which appeared in the region of the monomer 0-0 transition, have been analyzed (41). Rotational constants for the ground and excited states were found to be closely similar. They defined an average intermolecular separation of 3.79 ± 0.07 Å. For the electronically excited state, the ro-vibrational structure indicated a weakly anisotropic IPS, and immeasurably small spin-rotation splittings (Dubernet et al's (38) case (B)). The B state levels were identified as the origin $(0,0^0,0)$, a Π- bend $(0,1^1,0)$, and a Σ- bend $(0,1^0,0)$. In

22

the free-rotor limit these levels would be degenerate, and the transition to the origin forbidden. A fit of Eq(1) to the hindered rotor spacings yielded radially averaged angular potential parameters of C_1=8.6 and C_2=0.67 cm^{-1}. Hence, the equilibrium geometry is linear, and there is a 17 cm^{-1} barrier to internal rotation. In contrast with OH-Ar and OH-Ne, the CN-Ne IPS was almost unaffected by electronic excitation. This conclusion was drawn from the transition intensities, and the fact that the CN-Ne origin occurs exactly at the position of the forbidden CN Q(0) line.

4. References

1. T. Ishiwata and I. Tanaka, Laser Chem. $\underline{7}$, 79 (1987)

2. M. Nota, A. J. Bouvier, R. Bascis, A. Bouvier, P. Crozet, S. Churassy and J. B. Koffend, J. Chem. Phys. $\underline{91}$, 5903 (1989)

3. J. Tellinghuisen, S. Fei, X. Zheng, and M. C. Heaven, Chem. Phys. Lett. $\underline{176}$, 373 (1991)

4. L. J. van der Burgt and M. C. Heaven, J. Chem. Phys. $\underline{89}$, 2768 (1988)

5. J. Tellinghuisen, A. R. Whyte, and L. F. Phillips, J. Phys. Chem. $\underline{88}$, 6084 (1984)

6. J. Tellinghuisen and L. F. Phillips, J. Phys. Chem. $\underline{90}$, 5108 (1986)

7. A. L. Guy, K. S. Viswanathan, A. Sur, and J. Tellinghuisen, Chem. Phys. Lett. $\underline{73}$, 582 (1980)

8. J. Tellinghuisen, Chem. Phys. Lett. $\underline{99}$, 373 (1983)

9. J. Tellinghuisen, Adv. Phys. Chem. $\underline{60}$, 299 (1985)

10. S. Gerstenkorn and P. Luc, *"Atlas du Spectre d'Absorption de la Molécule d'Iodide"*, Laboratorie Amie Cotton, CNRS II, Orsay, France, (1977)

11. X. Zheng, S. Fei, M. C. Heaven, and J. Tellinghuisen, J. Mol. Spec. $\underline{149}$, 399 (1991)

12. X. Zheng, S. Fei, M. C. Heaven, and J. Tellinghuisen, J. Chem. Phys. Accepted, December 1991

13. P. B. Beeken, E. A. Hanson, and G. W. Flynn, J. Chem. Phys. $\underline{78}$, 5892 (1983)

14. R. Böhling, J. Langen, and U. Schurath, Chem. Phys. 130, 419 (1989)

15. M. Macler, J. P. Nicolai, and M. C. Heaven, J. Chem. Phys. 91, 674 (1989)

16. M. Macler and M. C. Heaven, Chem. Phys. 151, 219 (1990)

17. M. Mandich, P. Beeken, and G. W. Flynn, J. Chem. Phys. 77, 702, (1982)

18. P. B. Beeken, M. Mandich, and G. W. Flynn, J. Chem. Phys. 76, 5995, (1982)

19. J. Langen, K.-P. Lodeman, and U. Schurath, Chem. Phys. 112, 393 (1987)

20. V. E. Bondybey and C. Fletcher, J. Chem. Phys. 64, 3615 (1976)

21. V. E. Bondybey and L. E. Brus, J. Chem. Phys. 62,620 (1075); 64, 3724 (1976)

22. J. P. Nicolai and M. C. Heaven, J. Chem. Phys. 87, 3304 (1987)

23. see J. C. D. Brand and A. R. Hoy, Appl. Spectrosc. Rev. 23, 285, (1987) and references therein.

24. B. Guo and J. Tellinghuisen, J. Mol. Spectrosc. 127, 222 (1988).

25. R. H. Lipson, A. R. Hoy, and N. McDonald, J. Mol. Spctrosc. 142, 24 (1990)

26. A. R. Hoy, K. J. Jordan, and R. H. Lipson, J. Phys. Chem. 95, 611 (1991)

27. J. P. Nicolai, L. J. van der Burgt, and M. C. Heaven, Chem. Phys. Lett. 115, 486 (1985)

28. M. Macler, M. Erickson, and M. C. Heaven, J. Phys. Chem. Submitted, December 1991

29. M. C. Heaven, Ann. Rev. Phys. Chem. 43 (1992)

30. M. J. McQuaid, J. L. Gole, and M. C. Heaven, J. Chem. Phys. $\underline{92}$, 2733 (1990)

31. W. M. Fawzy and M. C. Heaven, J. Chem. Phys. $\underline{92}$, 909 (1990)

32. J. Goodman and L. E. Brus, J. Chem. Phys, $\underline{67}$,4858 (1977)

33. J. M. Bowman, B. Gazdy, P. Schafer, and M. C. Heaven, J. Phys. Chem. $\underline{94}$, 2226 (1990); $\underline{94}$, 8858 (1990)

34. A. Degli Esposti and H.-J. Werner, J. Chem. Phys. $\underline{93}$, 3351 (1990)

35. S. K. Kulkarni, Y. Lin, and M. C. Heaven, Chem. Phys. Lett. $\underline{167}$, 597 (1990)

36. Y. Lin, S. K. Kulkarni, and M. C. Heaven, J. Phys. Chem. $\underline{94}$, 1720 (1990)

37. Y. Lin, *"Spectroscopic and Dynamic Studies of Br_2 and Open-Shell van der Waals Complexes"*, Ph. D. Thesis, Emory University (1990)

38. M.-L. Dubernet, D. Flower, and J. M. Hutson, J. Chem. Phys. $\underline{94}$, 7602 (1991)

39. L. E. Brus and V. E. Bondybey, J. Chem. Phys. $\underline{63}$, 786 (1975)

40. T. Bergeman, P. Erman, Z. Haratym, and M. Larsson, Physica Scripta, 23, $\underline{45}$ (1981)

41. Y. Lin and M. C. Heaven, J. Chem. Phys. $\underline{84}$, 5765 (1991)

5. Publications Resulting from AFOSR Support

1. "Electronic Spectroscopy of the ArOH and ArOD Complexes", W. Fawzy and M.C. Heaven, J. Chem. Phys. , 92, 909 (1990).

2. "Spectroscopy of the AlAr van der Waals Complex: Rotationally Resolved B-X Electronic Transitions", M. J. McQuaid, J. L. Gole and M. C. Heaven, J. Chem. Phys., 92, 2733 (1990).

3. "Rotationally Resolved Electronic Spectra for the Ne-OH and Ne-OD van der Waals Complexes", Y. Lin, S. K. Kulkarni, and M. C. Heaven, J. Phys. Chem., 94, 1720 (1990).

4. "A Potential Energy Surface for Ar-OH($^2\Sigma$) and Ar-OD($^2\Sigma$): Fitting and Assigning Experimental Data with Rigorous Theory", J.M. Bowman, B. Gazdy, P. Schafer, and M.C. Heaven, J. Phys. Chem., 94, 2226 (1990).

5. "Fluorescence Decay and Non-Radiative Relaxation Dynamics of the $A^2\Sigma^+$ States of OH-Ar and OD-Ar", S.K. Kulkarni, Y. Lin, and M.C. Heaven, Chem. Phys. Lett., 167, 597 (1990).

6. "Spectroscopy and Relaxation Dynamics of Metastable Electronically Excited States of Iodine in Rare Gas Matrices", Macler and M. C. Heaven, Chem. Phys., 151, 219 (1991).

7. "Observation and Analysis of the D'-A' Transition of I$_2$ in a Free-Jet Expansion", J. Tellinghuisen, X. Zheng, S. Fei, and M. C. Heaven, Chem. Phys. Lett., 176, 373 (1991).

8. "Observation and Analysis of the CN-Ne B-X Transition", Y. Lin and M. C. Heaven, J. Chem. Phys., 94, 5765 (1991).

9. "Observation and Analysis of the β - A Transition of I2 in a Free-Jet Expansion", X. Zheng, S. Fei, M. C. Heaven, and J. Tellinghuisen, J. Mol. Spec., <u>149</u>, 399 (1991).

10. "Spectroscopy of Metastable Species in a Free-Jet Expansion: The $D' \leftarrow A'$ Transition of I_2", X. Zheng, S. Fei, M. C. Heaven, and J. Tellinghuisen, J. Chem. Phys., in press.

11. "Electronic Spectroscopy and Fluorescence Decay Dynamics of Matrix Isolated IBr", M. Macler, M. Erickson, and M. C. Heaven, J. Phys. Chem., Submitted, December 1991.

12. "Spectroscopy and Dynamics of Open-Shell van der Waals Molecules", M. C. Heaven, Ann. Rev. Phys. Chem., <u>43</u>, xxx (1992)